

REDUCING TRAINING COMPLEXITY IN EMPIRICAL QUADRATURE-BASED MODEL REDUCTION VIA STRUCTURED COMPRESSION

BJÖRN LILJEGREN-SAILER*

Abstract. Model order reduction seeks to approximate large-scale dynamical systems by lower-dimensional reduced models. For linear systems, a small reduced dimension directly translates into low computational cost, ensuring online efficiency. This property does not generally hold for nonlinear systems, where an additional approximation of nonlinear terms –known as complexity reduction– is required. To achieve online efficiency, empirical quadrature and cell-based empirical cubature are among the most effective complexity reduction techniques. However, existing offline training algorithms can be prohibitively expensive because they operate on raw snapshot data of all nonlinear integrands associated with the reduced model. In this paper, we introduce a preprocessing approach based on a specific structured compression of the training data. Its key feature is that it scales only with the number of collected snapshots, rather than additionally with the reduced model dimension. Overall, this yields roughly an order-of-magnitude reduction in offline computational cost and memory requirements, thereby enabling the application of the complexity reduction methods to larger-scale problems. Accuracy is preserved, as indicated by our error analysis and demonstrated through numerical examples.

AMS subject classifications.

Key words. model reduction; nonlinear model reduction; hyper-reduction; complexity reduction; structure-preserving; empirical quadrature; empirical cubature

Let a *truth* nonlinearity $\mathbf{f} : \mathbb{R}^N \rightarrow \mathbb{R}^N$ of high dimension N be given. We define its projected counterpart by

$$\mathbf{f}_r : \mathbb{R}^{N_r} \rightarrow \mathbb{R}^{N_r}, \quad \mathbf{f}_r : \mathbf{x}_r \mapsto \mathbf{W}^T \mathbf{f}(\mathbf{V} \mathbf{x}_r),$$

where $\mathbf{W}, \mathbf{V} \in \mathbb{R}^{N, N_r}$ induce a projection onto a low dimension $N_r \ll N$. Although the nonlinearity \mathbf{f}_r is low-dimensional its evaluation cost is –in the general nonlinear case– not independent of the truth dimension N . This is a typical scenario, specifically when nonlinear partial differential equations are approximated using projection-based model order reduction methods. In order to avoid the high evaluation costs during time-critical online computations, a complexity-reduction (also known as hyper-reduction) is performed. In an offline training phase a complexity-reduced nonlinearity

$$\mathbf{f}_c : \mathbb{R}^{N_r} \rightarrow \mathbb{R}^{N_r}, \quad \text{with } \mathbf{f}_c \approx \mathbf{f}_r$$

is constructed as a surrogate for \mathbf{f}_r . Online efficiency is achieved by imposing some sort of sparsity on the approximation, which avoids the evaluation costs to scale with the full dimension N . One can distinguish two classes of complexity-reduction methods.

In this work, we focus on those that adopt the *project-then-approximate* paradigm, and our goal is to enhance the offline training algorithms associated with these methods. The empirical quadrature [7, 15, 21] and the cell-based

*Radon Institute for Computational and Applied Mathematics (RICAM), Austrian Academy of Sciences, Altenberger Str. 69, 4040 Linz, Austria (Corresponding author: bsailer@ricam.oeaw.ac.at).

empirical cubature [8, 2, 9] (also known as ECSW [4]) are the principal representatives of project-then-approximate techniques. As the name suggests, the training phase of these methods seeks to approximate the projected nonlinearity directly. This approach typically yields a complexity reduction with high fidelity and robust online performance. Moreover, an additional advantage of this class of methods is that fundamental structural properties –such as dissipative relations or a conservation law interpretation– can be preserved through simple variational arguments in many relevant settings.

The second class of complexity-reduction methods, referred to as *approximate-then-project* methods, generally exhibits less robust online performance, particularly in applications where the aforementioned structural properties play a critical role [1, 18, 22]. Nonetheless, they seem to be applied more in practice, specifically the Empirical Interpolation Method and its discrete variant [5, 6]. The primary advantage lies in the availability of highly efficient offline training procedures that operate exclusively on compressed training data.

To the best of the author’s knowledge, no comparably well-scaled algorithm for training project-then-approximate methods has been proposed to date. In this work, we aim to address this gap by introducing a preprocessing step for these methods that leverages the structure inherent in the respective training problems and which reduces the computational costs significantly.

Organization of the paper. The structure of the paper is as follows. The spatial discretization and the model order reduction setting for this paper is established in Section 1. The complexity reduction ansatz itself is presented in Section 2. Section 3 reviews existing training methods for complexity reduction. Our proposed preprocessing approach based on a structured compression is then introduced. The general data compression strategy is derived in Section 4, while Section 5 develops related structured representations tailored to our specific training problems. Section 6 provides an error analysis, including an a posteriori bound. Finally, Section 7 presents numerical performance tests demonstrating the efficiency of our proposed data compression approach and the reliability of the a posteriori bound.

Notation. Matrices, vectors, and scalars are indicated by capital boldfaced, small boldfaced, and normal letters, respectively, whereby vector expressions always refer to column vectors. The norm $\|\cdot\|$ refers to the spectral norm for matrices and to the Euclidean norm for vectors, respectively. We write $\|\cdot\|_{\text{F}}$ for the Frobenius norm, i.e., $\|\mathbf{Q}\|_{\text{F}}^2 = \sum_{i=1}^M \sum_j^N |q_{ij}|^2$ for any $\mathbf{Q} \in \mathbb{R}^{M,N}$. The symbol ‘ \circ ’ denotes the Hadamard product, which is the elementwise multiplication operator between two vectors of the same dimension. Given a vector $\mathbf{v} \in \mathbb{R}^N$, we write $\text{diag}(\mathbf{v}) \in \mathbb{R}^{N,N}$ for the diagonal matrix with diagonal entries given by the entries of \mathbf{v} , and $[\mathbf{v}]_i$ for its i -th entry of the vector. Moreover, the cardinality of any finite set I_c is denoted by $|I_c|$.

1. Setting for the paper.

1.1. Model hierarchy in the algebraic setting. Consider an input-output map $\mathbf{u} \mapsto \mathbf{y}$ described in terms of the dynamical system

$$\frac{d}{dt} \mathbf{x}(t) = \mathbf{f}(\mathbf{x}(t)) + \mathbf{A}\mathbf{x}(t) + \mathbf{B}\mathbf{u}(t), \quad \mathbf{y}(t) = \mathbf{C}\mathbf{x}(t)$$

for time $t \in [0, T]$ and system matrices $\mathbf{A} \in \mathbb{R}^{N,N}$, $\mathbf{B} \in \mathbb{R}^{N,p}$, $\mathbf{C} \in \mathbb{R}^{q,N}$. We assume $p, q \ll N$, which motivates the use of model reduction. The $\mathbf{f} : \mathbb{R}^N \rightarrow \mathbb{R}^N$ describes the truth nonlinearity and the latter system is denoted as the full order model (FOM), which can be closed by appropriate initial conditions.

In the nonlinear case, the model reduction consists of two steps. Firstly, the model order reduction is performed, using reduction bases $\mathbf{W}, \mathbf{V} \in \mathbb{R}^{N,N_r}$ and $N_r \ll N$. Assuming the usual bi-orthogonality assumption $\mathbf{W}^T \mathbf{V} = \mathbf{I}$ holds, the reduced order model (ROM) is then given as the following projection of the FOM,

$$\frac{d}{dt} \mathbf{x}_r(t) = \mathbf{f}_r(\mathbf{x}_r(t)) + \mathbf{A}_r \mathbf{x}_r(t) + \mathbf{B}_r \mathbf{u}(t), \quad \mathbf{y}_r(t) = \mathbf{C}_r \mathbf{x}_r(t),$$

with reduced matrices $\mathbf{A}_r = \mathbf{W}^T \mathbf{A} \mathbf{V}$, $\mathbf{B}_r = \mathbf{W}^T \mathbf{B}$, $\mathbf{C}_r = \mathbf{C} \mathbf{V}$. The second step, termed complexity reduction, involves approximating the projected nonlinearity $\mathbf{f}_r : \mathbf{x}_r \mapsto \mathbf{W}^T \mathbf{f}(\mathbf{V} \mathbf{x}_r)$ by a complexity-reduced nonlinearity $\mathbf{f}_c : \mathbb{R}^{N_r} \rightarrow \mathbb{R}^{N_r}$. Replacing the projected nonlinearity in the ROM with \mathbf{f}_c yields the complexity-reduced model (CROM). In this paper, we focus primarily on the complexity reduction step, and, more specifically, on its training phase.

1.2. Projected nonlinearity in the function space setting. The underlying function space perspective is also relevant for our approach. We assume that the FOM arises from the discretization of a partial differential equation posed on a bounded spatial domain $\Omega \subset \mathbb{R}^d$, with $d \in \{1, 2, 3\}$. For simplicity, we restrict ourselves to a standard finite element setting and assume that \mathbf{f} in the FOM corresponds to a scalar-valued function $f : \Omega \rightarrow \mathbb{R}$.

Let \mathcal{W} and \mathcal{V} denote the test and trial spaces of the finite element discretization, respectively, both of dimension N . The basis of \mathcal{W} is given by $\varphi^1, \dots, \varphi^N : \Omega \rightarrow \mathbb{R}$. We denote the FOM state by $x : [0, T] \rightarrow \mathcal{V}$ for $t \in [0, T]$, and assume that the truth nonlinearity $\mathbf{f} : \mathbb{R}^N \rightarrow \mathbb{R}^N$ can be written as

$$[\mathbf{f}(\mathbf{x}(t))]_n = \int_{\Omega} f(x(t)) \varphi^n d\xi, \quad \text{for } n = 1, \dots, N,$$

where \mathbf{x} denotes the coordinate representation of x in the FOM basis. The ROM is obtained by projecting the FOM onto reduced spaces $\mathcal{W}_r \subset \mathcal{W}$ and $\mathcal{V}_r \subset \mathcal{V}$, with $\dim(\mathcal{W}_r) = \dim(\mathcal{V}_r) = N_r$. Let the ROM state $x_r : [0, T] \rightarrow \mathcal{V}_r$ approximate x . The ROM nonlinearity $\mathbf{f}_r : \mathbb{R}^{N_r} \rightarrow \mathbb{R}^{N_r}$ is then defined by

$$[\mathbf{f}_r(\mathbf{x}_r(t))]_n = \int_{\Omega} f(x_r(t)) \varphi_r^n d\xi, \quad \text{for } n = 1, \dots, N_r,$$

where $\varphi_r^1, \dots, \varphi_r^{N_r}$ form a basis of \mathcal{W}_r , and \mathbf{x}_r is the coordinate representation of x_r in the ROM basis.

REMARK 1.1. *The continuous setting described here relates to the algebraic framework in Section 1.1 as follows: the columns of the reduction basis \mathbf{W} are the coordinate representations of the test functions $\varphi_r^1, \dots, \varphi_r^{N_r}$ in the FOM space \mathcal{W} . Likewise, the columns of \mathbf{V} represent the coordinates of \mathcal{V}_r .*

2. Complexity reduction ansatz. A complexity reduction method constructs a cheaper-to-evaluate surrogate for the projected nonlinearity \mathbf{f}_r . In the

case of the project-then-approximate methods this is done based on a *truth sum representation* of the nonlinearity. We shortly introduce the empirical quadrature and the empirical cubature setting in Sections 2.1-2.2. As the two approaches share many similarities, we then go over to a more generic setting in Section 2.3 to formalize the respective training problem in the algebraic setting.

2.1. Empirical quadrature. In empirical quadrature, the truth representation is defined by a general quadrature rule with points ξ_m and weights $\tilde{\omega}_m$ for $m = 1, \dots, M_{\text{quad}}$. We assume that the FOM nonlinearity is evaluated using this truth quadrature, i.e.,

$$[\mathbf{f}(\mathbf{x}(t))]_n = \tilde{b}^{\text{quad}}(f(x(t)), \varphi^n) := \sum_{m=1}^{M_{\text{quad}}} \tilde{\omega}_m f(x(t, \xi_m)) \varphi^n(\xi_m)$$

for $n = 1, \dots, N$. By construction the \tilde{b}^{quad} is a bilinear form. Here and in the following, we use the same symbol for the state $x : [0, T] \rightarrow \mathcal{V}$ and its real-valued counterpart $x : [0, T] \times \Omega \rightarrow \mathbb{R}^d$, to keep the notation concise. The projected nonlinearity allows for a similar representation, given as

$$[\mathbf{f}_r(\mathbf{x}_r(t))]_n = \tilde{b}^{\text{quad}}(f(x_r(t)), \varphi_r^n) = \sum_{m=1}^{M_{\text{quad}}} \tilde{\omega}_m f(x_r(t, \xi_m)) \varphi_r^n(\xi_m)$$

for $n = 1, \dots, N_r$. It is important to note that the truth nonlinearity typically exhibits sparsity, meaning that most summands in the sum representation of $[\mathbf{f}(\cdot)]_n$ are zero. However, no sparsity can generally be expected for \mathbf{f}_r , so its evaluation typically scales with $M_{\text{quad}} \geq N$.

As a remedy, empirical quadrature can be used. The idea of the latter is to replace the truth bilinear form \tilde{b}^{quad} by a complexity-reduced version $\tilde{b}_c^{\text{quad}}$. The resulting complexity-reduced nonlinearity \mathbf{f}_c then reads

$$[\mathbf{f}_c(\mathbf{x}_r(t))]_n = \tilde{b}_c^{\text{quad}}(f(x_r(t)), \varphi_r^n) := \sum_{m \in I_c} \omega_m f(x_r(t, \xi_m)) \varphi_r^n(\xi_m)$$

for $n = 1, \dots, N_r$. The subset $I_c \subset \{1, \dots, M_{\text{quad}}\}$ and weights $\omega_m \geq 0$, $m \in I_c$, are subject to an offline training. Following [15], we consider the following training problem:

Given snapshots $x^1, \dots, x^K \subset \mathcal{V}$ of the FOM solution and $M_c \ll M_{\text{quad}}$, and choosing and a regularization (reg.), solve

$$\min_{\substack{I_c, |I_c| \leq M_c \\ \omega_m \geq 0, m \in I_c}} \sum_{k=1, \dots, K} \left\| \left(\sum_{m \in I_c} \omega_m f(x^k(\xi_m)) \varphi_r^n(\xi_m) \right) - \tilde{b}^{\text{quad}}(f(x^k), \varphi_r^n) \right\|^2 \quad (+\text{reg.})$$

REMARK 2.1. Note that snapshots $x^k \in \mathcal{V}$ of the FOM are used in the training problem. It might seem more natural to use snapshots restricted to the reduced space \mathcal{V}_r instead. However, the evaluation with projected training data requires additional computational costs with very minor impact on the result of the training, cf. [15, 8]. The same can be said and done for other project-then-approximate complexity reduction methods.

2.2. Cell-based empirical cubature. In the standard finite element setting, the domain Ω is partitioned into non-overlapping cells $\Omega_1, \dots, \Omega_{M_{\text{cells}}}$. The (cell-based) empirical cubature approach exploits a sum representation of \mathbf{f} induced by this partitioning. Thus, it holds

$$[\mathbf{f}(\mathbf{x}(t))]_n = \tilde{b}^{\text{cells}}(f(x(t)), \varphi^n) := \sum_{m=1}^{M_{\text{cells}}} \int_{\Omega_m} f(x(t)) \varphi^n d\xi,$$

for $n = 1, \dots, N$. Most summands vanish due to the small local support of the test functions. The projected nonlinearity admits a similar representation, given by

$$[\mathbf{f}_r(\mathbf{x}_r(t))]_n = \tilde{b}^{\text{cells}}(f(x_r(t)), \varphi_r^n) = \sum_{m=1}^{M_{\text{cells}}} \int_{\Omega_m} f(x_r(t)) \varphi_r^n d\xi,$$

for $n = 1, \dots, N_r$. Here, generally no summands vanish, so the evaluation cost scales with M_{cells} rather than N_r .

Complexity reduction is achieved by replacing \tilde{b}^{cells} with a sparse bilinear form $\tilde{b}_c^{\text{cells}}$. The resulting approximation \mathbf{f}_c then reads

$$[\mathbf{f}_c(\mathbf{x}_r(t))]_n = \tilde{b}_c^{\text{cells}}(f(x_r(t)), \varphi_r^n) := \sum_{m \in I_c} \omega_m \int_{\Omega_m} f(x_r(t)) \varphi_r^n d\xi,$$

for $n = 1, \dots, N_r$. The subset $I_c \subset \{1, \dots, M_{\text{cells}}\}$ together with the weights $\omega_m \geq 0$, $m \in I_c$, are determined by the following training problem; cf. [8]:

Given snapshots $x^1, \dots, x^K \subset \mathcal{V}$ of the FOM solution and $M_c \ll M_{\text{cells}}$ and choosing regularization (reg), solve

$$\min_{\substack{I_c, |I_c| \leq M_c \\ \omega_m \geq 0, m \in I_c \\ n=1, \dots, N_r}} \left\| \left(\sum_{m \in I_c} \omega_m \int_{\Omega_m} f(x^k) \varphi_r^n d\xi \right) - \tilde{b}^{\text{cells}}(f(x^k), \varphi_r^n) \right\|^2 \quad (+\text{reg.})$$

2.3. Generic and algebraic setting. In slight generalization to the empirical quadrature and cubature setting, let us assume that a truth sum representation of projected nonlinearity \mathbf{f}_r is given by

$$[\mathbf{f}_r(\bar{x}_r)]_n = \tilde{b}^*(f(\bar{x}_r), \varphi_r^n) := \sum_{m=1}^M \tilde{\omega}_m \beta_*^m(f(\bar{x}_r), \varphi_r^n), \quad \text{for } n = 1, \dots, N_r$$

and $\bar{x}_r \in \mathcal{V}_r$. We additionally pose the assumption that each of the localized bilinear terms β_*^m has a low computational cost. This then motivates a complexity reduction based on an approximation of \tilde{b}^* with a sparse sum. The respective complexity-reduced nonlinearity \mathbf{f}_c becomes

$$[\mathbf{f}_c(\bar{x}_r)]_n := \tilde{b}_c^*(f(\bar{x}_r), \varphi_r^n) := \sum_{m \in I_c} \omega_m \beta_*^m(f(\bar{x}_r), \varphi_r^n), \quad \text{for } n = 1, \dots, N_r.$$

The subset $I_c \subset \{1, \dots, M\}$ and weights $\omega_m \geq 0$ of the complexity reduction are subject to the following training problem:

infeasible and unnecessary. Consequently, greedy strategies are employed in practice. We adopt the Orthogonal Matching Pursuit [20, 3], which is well-suited to the structure of our training problem. The core idea is to alternate between expanding the index set I_c through a greedy search and computing optimal weights for the fixed set. A possible implementation is sketched in [Algorithm 3.1](#).

Algorithm 3.1 Orthogonal Matching Pursuit for offline training

- 1: **Input:** Training data $(\mathcal{A}, \mathbf{g})$, dimension set M_c
- 2: **Output:** Sparse weights \mathbf{u}^{M_c} , residual $\sqrt{F(\mathbf{u}^{M_c})}$
- 3: Define $F(\mathbf{u}) = \|\mathcal{A}\mathbf{u} - \mathbf{g}\|^2$, with gradient $\nabla F = 2\mathcal{A}^T(\mathcal{A}\mathbf{u} - \mathbf{g})$
- 4: Initialize $I_0 = \emptyset$, $\mathbf{u}^0 = \mathbf{0}$
- 5: **for** $k = 1 : M_c$ **do**
- 6: Define set of candidates $I_c = \{1, \dots, M\} \setminus I_{k-1}$
- 7: Find $j_{\max} = \arg \max_{j \in I_c} -[\nabla F(\mathbf{u}^{k-1})]_j$
- 8: Set $I_k = I_{k-1} \cup \{j_{\max}\}$
- 9: Solve $\min_{\mathbf{u}=[\omega_1, \dots, \omega_M]^T} F(\mathbf{u})$
s.t. $\omega_i \geq 0$ for $i \in I_k$, $\omega_j = 0$ for $j \notin I_k$
- 10: **end for**
- 11: Compute residual $\sqrt{F(\mathbf{u}^{M_c})}$

Even with the adoption of a greedy procedure, offline training based on [Problem 1](#) remains highly computationally demanding, as it operates directly on raw snapshot data. This data typically exhibits near-linear dependencies among equations and the equation number scales with KN_r .

The linear dependencies can cause convergence issues for certain greedy algorithms. While such issues can be mitigated using standard compression techniques [26], the computational cost poses a more critical challenge, as noted by several authors and shown in the numerical section. In [15], compression of the training data is proposed as a remedy. However, since this compression is applied to the raw solution manifold, the approach still scales with the full complexity of [Problem 1](#). To make it feasible, partitioned SVD –an inexact compression technique– is suggested. Similarly, [14] advocates the use of randomized SVD. Other works rely on massive parallelization [7, 12], enabling the treatment of large-scale problems given sufficient computational resources. While effective, these approaches may still become prohibitively expensive as dimensions grow.

In contrast, we pursue a different strategy: reducing the complexity of the training problem itself through structured data compression. In principle, our approach can be combined with parallelization or other large-scale techniques mentioned above. However, the focus of this paper is exclusively on the pre-processing strategy.

4. Preprocessing by structured data compression. The basic idea of our preprocessing approach is to approximate the solution manifold matrix $\tilde{\mathbf{A}}$ in [\(2.2\)](#). Note that $\tilde{\mathbf{A}}$ consists of raw snapshot data, and its row dimension scales with $N_r K$, i.e., with the ROM dimension. Since the matrix is dense, it can

become very large in practical settings, potentially too large to fit into memory.

To address this and reduce the associated computational overhead, we propose preprocessing the training data through compression, resulting in a data-compressed training problem. More specifically, we construct a structured low-rank approximation of $\tilde{\mathbf{A}}$ based on a suitable factorization of the data. The compression is applied exclusively along the snapshot dimension K . The advantage of this structured approach is that it eliminates operations scaling with KN_r , i.e., the row dimension of $\tilde{\mathbf{A}}$, and instead achieves scaling with K only. The structured compression problem underlying our approach is outlined in Section 4.1. Further required technical results and an abstract algorithmic implementation of the proposed preprocessing itself are provided in Section 4.2.

4.1. The preprocessing problem. When K is compressed to $K_t \ll K$ in our approach, this yields a compressed solution manifold matrix \mathbf{A}_t and a respective compressed cost function of the form

$$(4.1) \quad \eta_t(\mathbf{u}) = \|\mathbf{A}_t(\mathbf{u} - \tilde{\mathbf{u}})\|, \quad \text{with } \mathbf{A}_t \in \mathbb{R}^{K_t N_r, M}.$$

The compressed training problem is then obtained replacing the exact cost function in [Problem 1](#) by its compressed counterpart.

PROBLEM 2. *Let η_t be as in (4.1) and let $\tilde{\mathbf{u}}$ denote the truth weights.*

$$\begin{aligned} \text{Solve} \quad & \min_{\substack{I_c \subset \{1, \dots, M\}, |I_c| \leq M_c \\ \mathbf{u} = [\omega_1, \dots, \omega_M]^T}} \eta_t(\mathbf{u})^2 + (\mathbf{d}^T(\mathbf{u} - \tilde{\mathbf{u}}))^2 \\ \text{s.t.} \quad & \omega_m \geq 0 \text{ for } m \in I_c, \quad \omega_{\bar{m}} = 0 \text{ for } \bar{m} \notin I_c, \end{aligned}$$

In what follows, we motivate and derive the compression step itself. We start by noting that $\tilde{\mathbf{A}} \in \mathbb{R}^{K N_r, M}$ is obtained from three-dimensional data and represents one matricization of a tensor in $\mathbb{R}^{K, N_r, M}$. For structured analysis, however, a different matricization is preferable, defined as

$$(4.2) \quad \begin{aligned} \tilde{\mathbf{C}} &= \begin{pmatrix} \beta_*^1(f(\mathbf{x}^1), \varphi_r^1) & \dots & \beta_*^1(f(\mathbf{x}^K), \varphi_r^1) \\ \beta_*^2(f(\mathbf{x}^1), \varphi_r^1) & \dots & \beta_*^2(f(\mathbf{x}^K), \varphi_r^1) \\ \vdots & \ddots & \vdots \\ \beta_*^M(f(\mathbf{x}^1), \varphi_r^1) & \dots & \beta_*^M(f(\mathbf{x}^K), \varphi_r^1) \\ \vdots & \ddots & \vdots \\ \beta_*^M(f(\mathbf{x}^1), \varphi_r^{N_r}) & \dots & \beta_*^M(f(\mathbf{x}^K), \varphi_r^{N_r}) \end{pmatrix} \\ &= \begin{pmatrix} \mathbf{a}^{1,1} & \dots & \mathbf{a}^{K,1} \\ \vdots & \ddots & \vdots \\ \mathbf{a}^{1,N_r} & \dots & \mathbf{a}^{K,N_r} \end{pmatrix}. \end{aligned}$$

By construction, $\tilde{\mathbf{C}}$ contains the same entries as $\tilde{\mathbf{A}}$. To fully exploit the underlying structure, we employ a factorization $\tilde{\mathbf{C}} = \mathbf{N}\hat{\mathbf{G}}$, where \mathbf{N} is a high-dimensional but sparse matrix encoding the constraints inherent in the data. As will be shown, the optimization can be reduced to a problem of the dimension of $\hat{\mathbf{G}}$, which is significantly lower than the dimension of $\tilde{\mathbf{A}}$. The derivation of the aforementioned factorization of $\tilde{\mathbf{C}}$ depends on the specific training problem; details are provided in Section 5. The structured training problem of our proposed preprocessing can now be stated.

PROBLEM 3. Let $\tilde{\mathbf{C}}$ from (4.2) be given in the structured form $\tilde{\mathbf{C}} = \mathbf{N}\hat{\mathbf{G}}$ with $\mathbf{N} \in \mathbb{R}^{N_r M, M_J}$ of full column rank and $\hat{\mathbf{G}} \in \mathbb{R}^{M_J, K}$. Let $K_t \ll \text{rank}(\tilde{\mathbf{C}})$.

$$\text{Solve} \quad \min_{\mathbf{G}_p, \text{rank}(\mathbf{G}_p) \leq K_t} \left\| \tilde{\mathbf{C}} - \mathbf{N}\mathbf{G}_p \right\|_F.$$

REMARK 4.1. Since the Frobenius norm of a matrix is invariant under any rearrangement of its entries, the following two best rank- k approximation problems minimize the same cost function:

$$\min_{\mathbf{C}_p, \text{rank}(\mathbf{C}_p) \leq K_t} \left\| \tilde{\mathbf{C}} - \mathbf{C}_p \right\|_F, \quad \text{and} \quad \min_{\mathbf{A}_p, \text{rank}(\mathbf{A}_p) \leq K_t} \left\| \tilde{\mathbf{A}} - \mathbf{A}_p \right\|_F,$$

given $\tilde{\mathbf{A}}$ and $\tilde{\mathbf{C}}$ as in (2.2) and (4.2), respectively. Similarly, Problem 3 shares the same cost function, but its admissible set is a subset of the best rank- k approximation problem for $\tilde{\mathbf{C}}$, which is of lower dimension. This reduction in dimension is the key to the efficiency of our approach.

4.2. Solving the compression problem. Structured problems of the form given in Problem 3 have been studied in the context of constrained principal component analysis [25, 24]. Among other results, connections to the standard best rank- k approximation problem have been established. The following lemma presents one such relation. For completeness, we also provide a brief proof sketch.

LEMMA 4.2. Let \mathbf{N} have the QR factorization $\mathbf{N} = \mathbf{Q}\mathbf{R}$. Then \mathbf{G}_p^* solves Problem 3, if and only if, $\mathcal{G}^* = \mathbf{R}\mathbf{G}_p^*$ solves

$$(4.3) \quad \min_{\mathcal{G}, \text{rank}(\mathcal{G}) \leq K_t} \left\| \mathbf{R}\hat{\mathbf{G}} - \mathcal{G} \right\|_F$$

Proof. Using $\tilde{\mathbf{C}} = \mathbf{N}\hat{\mathbf{G}}$, and exploiting the orthogonality of \mathbf{Q} together with the invariance of the Frobenius norm under orthogonal transformations, we obtain

$$\left\| \tilde{\mathbf{C}} - \mathbf{N}\mathbf{G}_p \right\|_F = \left\| \mathbf{Q}(\mathbf{R}\hat{\mathbf{G}} - \mathbf{R}\mathbf{G}_p) \right\|_F = \left\| \mathbf{R}\hat{\mathbf{G}} - \mathbf{R}\mathbf{G}_p \right\|_F = \left\| \mathbf{R}\hat{\mathbf{G}} - \mathcal{G} \right\|_F$$

for any choice of $\mathcal{G} = \mathbf{R}\mathbf{G}_p$. In particular, this holds for the minimizers \mathbf{G}_p^* and $\mathcal{G}^* = \mathbf{R}\mathbf{G}_p^*$ of the two minimization problems, from which the claim follows. \square

The problem (4.3) is a standard best rank- k approximation, which can be solved via singular value decomposition (SVD), see [11]. Consequently, together with Lemma 4.2, the following two corollaries can be deduced.

COROLLARY 4.3. Assume the conditions of Lemma 4.2 hold. Let $\sigma_1 \geq \dots \geq \sigma_{K_t} \geq \dots \geq 0$ denote the singular values of $\mathbf{R}\mathbf{G}_p^*$ in descending order. Let, further, $\sigma_{K_t} > \sigma_{K_t+1}$.

Then the solution to (4.3) is the truncated SVD $\mathcal{G}^* = \mathbf{U}_1^L \boldsymbol{\Sigma}_1 \mathbf{U}_1^R$, where $\boldsymbol{\Sigma}_1 = \text{diag}(\sigma_1, \dots, \sigma_{K_t})$, and $\mathbf{U}_1^L \in \mathbb{R}^{M_J, K_t}$, $\mathbf{U}_1^R \in \mathbb{R}^{K_t, K}$ contain the first K_t left and right singular vectors of $\mathbf{R}\mathbf{G}_p^*$, respectively.

The following corollary shows that the results of the standard best rank- k approximation extend naturally to our structured setting, provided the QR factorization of \mathbf{N} is available. In particular, it yields a compression bound in terms of the singular values of $\mathbf{R}\mathbf{G}_p^*$.

COROLLARY 4.4. Assume the conditions of Corollary 4.3. Then the solution of Problem 3 is given by $\mathbf{G}_p^* = \mathbf{R}^{-1} \mathbf{U}_1^L \boldsymbol{\Sigma}_1 \mathbf{U}_1^R$, and it fulfills the compression bound

$$\left\| \tilde{\mathbf{C}} - \mathbf{N} \mathbf{G}_p^* \right\|_{\text{F}} = \kappa, \quad \text{with } \kappa = \sqrt{\sum_{i>K_t} \sigma_i^2}.$$

Before proceeding, we would like to highlight two aspects required for the efficient implementation of the latter results. Firstly, the QR factorization of \mathbf{N} and the inverse \mathbf{R}^{-1} can be determined very efficiently in our setting, exploiting the specific structure of the training problem, cf. Section 5. Secondly, the low-rank approximations are identified with low-order matrices in an algorithmic implementation. For example, the solution $\mathbf{G}_p^* \in \mathbb{R}^{M_J, K}$ of the problem given as in Lemma 4.2 is identified with the low-order matrix

$$(4.4) \quad \mathbf{G}_t^* = \mathbf{R}^{-1} \mathbf{U}_1^L \boldsymbol{\Sigma}_1 \in \mathbb{R}^{M_J, K_t}, \quad \text{since } \mathbf{G}_p^* = \mathbf{G}_t^* \mathbf{U}_1^R,$$

choosing the basis \mathbf{U}_1^R in the identification. Similarly $\mathbf{N} \mathbf{G}_p^*$, which is the low-rank approximation of $\tilde{\mathbf{C}}$ we solve for in Problem 3, is identified with the low-order matrix $\mathbf{C}_t := \mathbf{N} \mathbf{G}_t^* \in \mathbb{R}^{N_r, M, K_t}$. The compressed solution manifold matrix \mathbf{A}_t defining Problem 2 is then obtained by an appropriate restructuring of \mathbf{C}_t . Our preprocessing procedure can now be summarized in Algorithm 4.1.

Algorithm 4.1 Structured preprocessing for offline training

- 1: **Input:** Structured snapshot data $\tilde{\mathbf{C}} = \mathbf{N} \hat{\mathbf{G}}$, compression dimension K_t
- 2: **Output:** Compressed matrix $\mathbf{A}_t \in \mathbb{R}^{K_t N_r, M}$, compression error κ
- 3: Determine^{*} QR factorization $\mathbf{N} = \mathbf{Q} \mathbf{R}$
- 4: Compute truncated SVD of $\mathbf{R} \hat{\mathbf{G}}$: $\mathcal{G}^* = \mathbf{U}_1^L \boldsymbol{\Sigma}_1 \mathbf{U}_1^R$, (with error κ)
- 5: Compute^{*} $\mathbf{G}_t^* = \mathbf{R}^{-1} \mathbf{U}_1^L$
- 6: Form \mathbf{A}_t from $\mathbf{C}_t := \mathbf{N} \mathbf{G}_t^*$ by permutation

^{*}exploiting the favorable matrix structure

REMARK 4.5. Since the matrix \mathbf{N} and its QR factors exhibit a highly favorable structure (cf. next section), the computational cost of Algorithm 4.1 is dominated by the SVD in step 4, which is performed on a matrix of significantly lower dimension than $\tilde{\mathbf{A}}$. The memory-critical assembly of $\tilde{\mathbf{A}}$ (or $\tilde{\mathbf{C}}$) is entirely avoided, as we operate directly on the factorized form of $\tilde{\mathbf{C}}$.

5. Structured representation of the training data. It remains to derive a structure-revealing factorization of $\tilde{\mathbf{C}}$ as postulated in Problem 3 and to analyze the structure of the resulting factors. In Section 5.1 we motivate the structural features inherent in the training data from a function-space point of view. The specific construction of the factorization is case-dependent. We first address the empirical quadrature case in Section 5.2, followed by a more general setting in Section 5.3, which also encompasses the empirical cubature case.

5.1. Structure induced by bilinear forms. Recall from the definition of $\tilde{\mathbf{C}}$ in (4.2) that the training data is composed of the terms $\beta_*^m (f(\mathbf{x}^k), \varphi_r^n)$

defined by localized bilinear forms

$$\beta_*^m : f(\mathcal{V}) \times \mathcal{V}_r \rightarrow \mathbb{R}, \quad m = 1, \dots, M.$$

The nonlinear manifold $f(\mathcal{V}) = \{y = f(x), x \in \mathcal{V}\}$ is induced by the nonlinearity f we would like to approximate. Not the full domain is considered, but only nonlinear snapshots related to the state snapshots $x^k \in \mathcal{V}$, cf. (2.1), i.e., the set

$$S_f = \{y = f(x) \text{ for } x \in \{x^1, \dots, x^K\}\} \subset f(\mathcal{V}).$$

Owing to the nonlinearity of the domain $f(\mathcal{V})$, no suitable representation of S_f exists that would permit the use of standard data compression techniques. To address this difficulty, we adopt a data representation based on the action of the nonlinearity on the bilinear forms β_*^m , rather than on the elements of S_f themselves. In this way, the analysis of the data structure is carried out from a dual-space perspective. More precisely, the factorization of the data matrix $\tilde{\mathbf{C}}$ assumed in [Problem 3](#) is derived from respective factorizations of the local bilinear forms β_*^m .

5.2. Structured data representation – empirical quadrature case. Considering the training problem for the empirical quadrature, the bilinear form $b^* = b^{\text{quad}}$ specifies to

$$b^*(f(\bar{x}_r), \varphi^n) = \sum_{m=1}^M \tilde{\omega}_m \beta_*^m(f(\bar{x}_r), \varphi_r^n) = \sum_{m=1}^M \tilde{\omega}_m f(\bar{x}_r(\xi_m)) \varphi_r^n(\xi_m)$$

using $M = M_{\text{quad}}$. In that case, the local bilinear forms β_*^m are separable already, in the sense that they can be divided into the two linear forms $f(\bar{x}_r) \mapsto f(\bar{x}_r(\xi_m))$ and $\varphi_r^n \mapsto \varphi_r^n(\xi_m)$. This simplifies our construction. Defining

$$\mathbf{g}^k = \begin{bmatrix} f(x^k(\xi_1)) \\ \vdots \\ f(x^k(\xi_M)) \end{bmatrix} \quad \text{for } k = 1, \dots, K, \quad \text{and} \quad \mathbf{p}^n = \begin{bmatrix} \varphi_r^n(\xi_1) \\ \vdots \\ \varphi_r^n(\xi_M) \end{bmatrix} \quad \text{for } n = 1, \dots, N_r,$$

we can write the sub-vectors $\mathbf{a}^{k,n}$ of (4.2) in the factorized form

$$\mathbf{a}^{k,n} = \mathbf{g}^k \circ \mathbf{p}^n \quad \text{for } k = 1, \dots, K, \quad n = 1, \dots, N_r.$$

Using the equality $\mathbf{g}^k \circ \mathbf{p}^n = \text{diag}(\mathbf{p}^n) \mathbf{g}^k$, the structure-revealing factorization assumed in [Problem 3](#) specializes in this case to

$$(5.1) \quad \begin{aligned} \tilde{\mathbf{C}} &= \mathbf{N} \hat{\mathbf{G}}, \quad \text{with} \quad \mathbf{N} \in \mathbb{R}^{MN_r, M}, \quad \hat{\mathbf{G}} \in \mathbb{R}^{M, K}, \\ &\text{given by} \quad \mathbf{N} = \begin{pmatrix} \text{diag}(\mathbf{p}^1) \\ \vdots \\ \text{diag}(\mathbf{p}^{N_r}) \end{pmatrix}, \quad \mathbf{G} = (\mathbf{g}^1 \quad \dots \quad \mathbf{g}^K). \end{aligned}$$

With reference to [Remark 4.5](#), we note the specific structure of \mathbf{N} in (5.1) and its implications for the computational complexity of [Algorithm 4.1](#). The columns of \mathbf{N} are orthogonal to each other. Thus a QR factorization of the matrix can be constructed analytically, choosing \mathbf{R} as the diagonal matrix with the reciprocal of the norms of the columns of \mathbf{N} on the diagonal.

5.3. Structured data representation – general case. Next, we study the more general setting, in which the local bilinear forms β_*^m are not separable themselves. Our strategy to deal with that is to decompose the local forms further into terms which are separable and then pursue with similar arguments as in the empirical quadrature case. In general, there may exist different decomposition of the β_*^m . Here, we suggest a construction based on the underlying FOM basis and the assumption that each basis function has a small local support.

Recall from our general setting in Section 1 that any ROM basis function φ_r^n is also an element of the FOM space. Therefore, any φ_r^n can be written as a linear combination $\varphi_r^n = \sum_{i=1}^N \lambda_i^n \varphi^i$ for $\varphi^1, \dots, \varphi^N$ given as the FOM basis. Further, due to the small local support assumption on the FOM basis, there exist index sets $J^m \subset \{1, \dots, M\}$ with small cardinalities $|J^m| \ll M$ such that for i fixed the linear forms $\beta_*^m(\cdot, \varphi^i) : f(\mathcal{V}) \rightarrow \mathbb{R}$ vanish for all $m \notin J^m$.

REMARK 5.1. *The cardinalities J^m are small for the typical model reduction settings. For instance, when the FOM originates from a discretization with nodal finite elements, J^m equals the number of nodes per cell. For example, linear finite elements on a simplex mesh in spatial dimension d yield $|J^m| = d + 1$, whereas piecewise constant ansatz functions lead to $|J^m| = 1$.*

Under the posed assumptions, we may write

$$\beta_*^m(\cdot, \varphi_r^n) = \sum_{i=1}^N \lambda_i^n \beta_*^m(\cdot, \varphi^i) = \sum_{i \in J^m} \lambda_i^n \beta_*^m(\cdot, \varphi^i) \quad \text{for } m = 1, \dots, M.$$

For any $x^k \in \mathcal{V}$ it then holds

$$\beta_*^m(f(x^k), \varphi_r^n) = \sum_{i \in J^m} \lambda_i^n \beta_*^m(f(x^k), \varphi^i) = (\hat{\mathbf{p}}^{n,m})^T \hat{\mathbf{g}}^{k,m},$$

for $\hat{\mathbf{p}}^{n,m} = [\lambda_i^n]_{i \in J^m} \in \mathbb{R}^{|J^m|}$ and $\hat{\mathbf{g}}^{k,m} = [\beta_*^m(f(x^k), \varphi^i)]_{i \in J^m} \in \mathbb{R}^{|J^m|}$. Define the sum of all cardinalities $M_J = \sum_{m=1}^M |J^m|$ and the concatenated vectors $\hat{\mathbf{p}}^n, \hat{\mathbf{g}}^k \in \mathbb{R}^{M_J}$ by

$$\hat{\mathbf{p}}^n = \begin{bmatrix} \hat{\mathbf{p}}^{n,1} \\ \vdots \\ \hat{\mathbf{p}}^{n,M} \end{bmatrix}, \quad n = 1, \dots, N_r \quad \text{and} \quad \hat{\mathbf{g}}^k = \begin{bmatrix} \hat{\mathbf{g}}^{k,1} \\ \vdots \\ \hat{\mathbf{g}}^{k,M} \end{bmatrix}, \quad k = 1, \dots, K.$$

Let $\mathbf{T} \in \mathbb{R}^{M_J, M}$ be the block-diagonal matrix that has $|J^m|$ one-entries on the m -th row. Then sub-vectors $\mathbf{a}^{k,n}$ of (4.2) can be written in the factorized form

$$\mathbf{a}^{k,n} = \beta_*(f(x^k), \varphi_r^n) = \mathbf{T} (\hat{\mathbf{p}}^n \circ \hat{\mathbf{g}}^k) = (\mathbf{T} \text{diag}(\hat{\mathbf{p}}^n)) \hat{\mathbf{g}}^k.$$

Summarizing, the structure-revealing factorization assumed in Problem 3 specializes in this case to

$$(5.2) \quad \begin{aligned} \tilde{\mathbf{C}} &= \mathbf{N} \hat{\mathbf{G}}, \quad \text{with} \quad \mathbf{N} \in \mathbb{R}^{MN_r, M_J}, \quad \hat{\mathbf{G}} \in \mathbb{R}^{M_J, K}, \\ &\text{given by } \mathbf{N} = \begin{pmatrix} \mathbf{T} \text{diag}(\hat{\mathbf{p}}^1) \\ \vdots \\ \mathbf{T} \text{diag}(\hat{\mathbf{p}}^{N_r}) \end{pmatrix}, \quad \hat{\mathbf{G}} = (\hat{\mathbf{g}}^1 \quad \dots \quad \hat{\mathbf{g}}^K). \end{aligned}$$

Note that the matrix \mathbf{N} in (5.2) separates into M blocks of column vectors, where each block spans a space that is orthogonal to each of the other ones. Exploiting that structure and since \mathbf{N} is sparse, it is possible to parallelize the calculation of the QR factorization efficiently, and the resulting \mathbf{R} then also has a favorable sparse block-diagonal structure.

As an alternative to the previous approach, we propose and employ a simplified compression strategy. Rather than applying data compression to the full matrix $\tilde{\mathbf{C}}$ in (5.2), we restrict it to the factor $\check{\mathbf{C}}$, defined as

$$(5.3) \quad \check{\mathbf{C}} := \check{\mathbf{N}} \hat{\mathbf{G}}, \quad \text{where } \check{\mathbf{N}} = \begin{pmatrix} \text{diag}(\hat{\mathbf{p}}^1) \\ \vdots \\ \text{diag}(\hat{\mathbf{p}}^{N_r}) \end{pmatrix}.$$

This construction satisfies $\tilde{\mathbf{C}} = \mathbf{T}_{\text{all}} \check{\mathbf{C}}$, where \mathbf{T}_{all} is a block-diagonal matrix consisting of N_r copies of \mathbf{T} . The QR factorization of $\check{\mathbf{N}}$ involves only column-wise operations and produces a diagonal QR factor \mathbf{R} , closely mirroring the structure encountered in empirical quadrature settings and can therefore be implemented in a similar manner.

REMARK 5.2. *Within the simplified compression approach, we approximate $\tilde{\mathbf{C}} \approx \mathbf{T}_{\text{all}} \check{\mathbf{C}}_t$, where $\check{\mathbf{C}}_t$ is obtained from using Algorithm 4.1 to the data of $\check{\mathbf{C}}$. Since $\|\mathbf{T}_{\text{all}}\| = \|\mathbf{T}\| = \max_m \sqrt{J_m}$ due to the block-structure, the approximation can be bounded as*

$$\|\tilde{\mathbf{C}} - \mathbf{T}_{\text{all}} \check{\mathbf{C}}_t\|_F = \|\mathbf{T}_{\text{all}}(\check{\mathbf{C}} - \check{\mathbf{C}}_t)\|_F \leq \|\mathbf{T}_{\text{all}}\| \|\check{\mathbf{C}} - \check{\mathbf{C}}_t\|_F = \left(\max_m \sqrt{J_m} \right) \|\check{\mathbf{C}} - \check{\mathbf{C}}_t\|_F,$$

where we used the fact that $\|\mathbf{T}_{\text{all}} \mathbf{M}\|_F \leq \|\mathbf{T}_{\text{all}}\| \|\mathbf{M}\|_F$ holds for any matrix \mathbf{M} independently of the specific structure of \mathbf{T}_{all} .

6. Error analysis of proposed preprocessing. In this section, we derive an effective a posteriori bound and an apriori bound that relate Problem 2 to Problem 1, thereby bounding the training error in our proposed preprocessing approach. For notational convenience, we introduce a prolonged representation of the compressed cost functional η_t . Instead of (4.1), we use the equivalent form

$$(6.1) \quad \eta_t(\mathbf{u}) = \|\mathbf{A}_p(\mathbf{u} - \tilde{\mathbf{u}})\|, \quad \text{with } \mathbf{A}_p \in \mathbb{R}^{KN_r, M},$$

where $\mathbf{A}_p \approx \tilde{\mathbf{A}}$ is chosen such that $\mathbf{A}_p = \tilde{\mathbf{Q}} \mathbf{A}_t$ for an orthogonal matrix $\tilde{\mathbf{Q}} \in \mathbb{R}^{KN_r, K_t N_r}$. Recall that the proposed preprocessing is based on a structured approximation of $\tilde{\mathbf{C}} \approx \mathbf{N} \mathbf{G}_p^*$, which is a permutation of $\tilde{\mathbf{A}}$. Moreover, the structured imposed by the factorization reduces the dimension of the problem. Due to the invariance of the Frobenius norm under matrix permutations, we have $\|\tilde{\mathbf{A}} - \mathbf{A}_p\|_F = \|\tilde{\mathbf{C}} - \mathbf{N} \mathbf{G}_p^*\|_F$, cf. Remark 4.1. Thus, the compression error

$$(6.2) \quad \kappa = \|\tilde{\mathbf{A}} - \mathbf{A}_p\|_F = \|\tilde{\mathbf{C}} - \mathbf{N} \mathbf{G}_p^*\|_F = \sqrt{\sum_{i>K_t} \sigma_i^2}$$

can be computed efficiently using Theorem 4.4, with \mathbf{N} , \mathbf{G}_p^* and the constant κ as defined in the corollary. The truncated singular values σ_i for $i > K_t$ are computed in the compression step of Algorithm 4.1 without incurring additional computational cost, since they are directly produced by the SVD.

THEOREM 6.1. Consider [Problem 1](#) and [Problem 2](#). Let \mathbf{A}_p be defined as in [\(6.1\)](#), and let κ be as in [\(6.2\)](#). Define d_{\min} as the smallest entry of \mathbf{d} , and assume $d_{\min} > 0$. Let \mathbf{u} be a feasible point of [Problem 2](#) such that $|\mathbf{d}^T(\mathbf{u} - \tilde{\mathbf{u}})| \leq \epsilon$ for some $\epsilon \geq 0$.

Then the cost function $\eta : \mathbf{u} \mapsto \|\tilde{\mathbf{A}}(\mathbf{u} - \tilde{\mathbf{u}})\|$ of [Problem 1](#) satisfies the following two bounds:

$$\eta(\mathbf{u}) \leq \eta_t(\mathbf{u}) + \kappa \|\mathbf{u} - \tilde{\mathbf{u}}\|, \quad (a \text{ posteriori bound})$$

$$\eta(\mathbf{u}) \leq \eta_t(\mathbf{u}) + \kappa \left(\frac{\sqrt{M_c}}{d_{\min}} (\epsilon + \mathbf{d}^T \tilde{\mathbf{u}}) + \|\tilde{\mathbf{u}}\| \right). \quad (a \text{ priori bound})$$

Proof. By definition of the cost functions, it follows

$$\begin{aligned} \eta(\mathbf{u}) &= \|\tilde{\mathbf{A}}(\mathbf{u} - \tilde{\mathbf{u}})\| \leq \|(\tilde{\mathbf{A}} - \mathbf{A}_p)(\mathbf{u} - \tilde{\mathbf{u}})\| + \|\mathbf{A}_p(\mathbf{u} - \tilde{\mathbf{u}})\| \\ &= \|(\tilde{\mathbf{A}} - \mathbf{A}_p)(\mathbf{u} - \tilde{\mathbf{u}})\| + \eta_t(\mathbf{u}) \leq \|(\tilde{\mathbf{A}} - \mathbf{A}_p)\| \|\mathbf{u} - \tilde{\mathbf{u}}\| + \eta_t(\mathbf{u}) \\ &\leq \|(\tilde{\mathbf{A}} - \mathbf{A}_p)\|_{\text{F}} \|\mathbf{u} - \tilde{\mathbf{u}}\| + \eta_t(\mathbf{u}) = \kappa \|\mathbf{u} - \tilde{\mathbf{u}}\| + \eta_t(\mathbf{u}), \end{aligned}$$

using the triangle inequality, sub-multiplicativity, and the consistency of the Frobenius norm with the spectral norm. This proves the a posteriori bound.

To proof the a priori bound, it remains to bound the term $\|\mathbf{u} - \tilde{\mathbf{u}}\|$ independently of \mathbf{u} . First note that due to the non-negativity of \mathbf{u} and \mathbf{d} , respectively, the one-norm of \mathbf{u} fulfills

$$\|\mathbf{u}\|_1 = \sum_{m \in I_c} |\omega_m| = \frac{1}{d_{\min}} \left(\sum_{m \in I_c} d_{\min} \omega_m \right) \leq \frac{1}{d_{\min}} (\mathbf{d}^T \mathbf{u}).$$

Since \mathbf{u} has at most M_c nonzero entries, it can be identified with a vector in \mathbb{R}^{M_c} , implying the norm relation $\|\mathbf{u}\| \leq \sqrt{M_c} \|\mathbf{u}\|_1$. Using the triangle inequality, we obtain

$$\begin{aligned} \|\mathbf{u} - \tilde{\mathbf{u}}\| &\leq \|\mathbf{u}\| + \|\tilde{\mathbf{u}}\| \leq \sqrt{M_c} \|\mathbf{u}\|_1 + \|\tilde{\mathbf{u}}\| \leq \frac{\sqrt{M_c}}{d_{\min}} (\mathbf{d}^T \mathbf{u}) + \|\tilde{\mathbf{u}}\| \\ &\leq \frac{\sqrt{M_c}}{d_{\min}} (\epsilon + \mathbf{d}^T \tilde{\mathbf{u}}) + \|\tilde{\mathbf{u}}\|. \end{aligned}$$

The a priori bound now follows from inserting the latter bound on $\|\mathbf{u} - \tilde{\mathbf{u}}\|$ into the a posteriori bound. \square

The first bound in [Theorem 6.1](#) provides a rigorous and computationally efficient estimate of the training error $\eta(\mathbf{u})$ that only depends on the compression error κ calculated in [Algorithm 4.1](#) but not on the full solution manifold matrix $\tilde{\mathbf{A}}$. The second bound offers an a priori estimate of the difference $\eta(\mathbf{u}) - \eta_t(\mathbf{u})$ that is independent of the argument \mathbf{u} . Concerning the constants in the latter we highlight the following: The regularization term in [Problem 2](#) enforces ϵ to be small, cf. the paragraph after [\(2.1\)](#). The quantities $\|\tilde{\mathbf{u}}\|$, d_{\min} , and $\mathbf{d}^T \tilde{\mathbf{u}}$ depend only on the FOM; in particular, $\mathbf{d}^T \tilde{\mathbf{u}}$ equals the volume of Ω under the setting of [Section 2](#).

7. Numerical performance study. The focus of our numerical studies is the comparison of complexity reduction without and with our proposed pre-processing via structured compression. We refer to the former as '**standard training**' and to the latter as '**compressed training**'. The compression is carried out using [Algorithm 4.1](#). Two representative nonlinear test problems are considered: one defined on a three-dimensional cube and another modeling a gas transport network; see Fig. 1 for the spatial domains.

The three-dimensional problem consists of a nonlinear reaction–diffusion equation. With sufficiently fine spatial meshes, this example can be scaled to high dimensions. It serves as the primary benchmark for demonstrating improvements in offline computational time and memory requirements.

The network problem models gas distribution in a pipeline network using cross-sectionally averaged nonlinear flow equations. We adopt the structure-preserving approximation from [\[19\]](#), which requires the use of the cell-based empirical cubature. In this example, we also demonstrate the tightness of the a posteriori error bound introduced in Section 6.

For both problems, we employ model order reduction based on proper orthogonal decomposition (POD). Time discretization is performed using the implicit Euler method, combined with a Newton method for solving the resulting algebraic systems. All computations were carried out on an Intel Xeon E-2136 processor with 6 cores and 48 GB of RAM using **Python** version 3.11.4, respectively **MATLAB** Version 9.14.0 (R2023a). Additional problem-specific parameter choices are provided below.

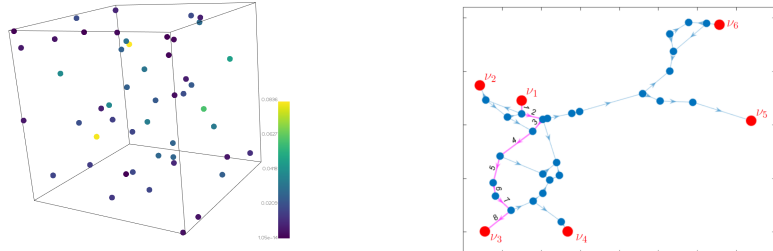


Fig. 1: Visualization of the spatial domains for both numerical benchmarks. Left: reaction-diffusion equation domain plus $M_c = 50$ trained empirical quadrature points; right: gas network topology from [\[19\]](#) with boundary nodes highlighted in red.

7.1. Three-dimensional reaction-diffusion equation. Let $\Omega \subset \mathbb{R}^3$ denote the unit cube with boundary $\partial\Omega$ and outward normal vector $\mathbf{n}_\Gamma : \partial\Omega \rightarrow \mathbb{R}^3$. Furthermore, define the subset of the boundary in the upper-right corner by $\Gamma_{\text{top,right}} = \{[\xi_1, \xi_2, \xi_3] \in \partial\Omega \mid \xi_1 = 1 \text{ or } \xi_3 = 1\}$, and the final time $t_{\text{end}} = 1.5$

We consider the reaction-diffusion equation for $t \in [0, t_{end}]$,

$$\begin{aligned} \frac{\partial}{\partial t} \rho(t, \xi) &= -\nabla(\mathbf{D} \nabla \rho(t, \xi)) + f(\rho(t, \xi)) & \text{for } \xi \in \Omega \\ (\mathbf{D} \nabla \rho(t, \xi)) \cdot \mathbf{n}_\Gamma(\xi) &= g_\Gamma(t, \xi; C) & \text{for } \xi \text{ on } \Gamma_{\text{top,right}} \\ (\mathbf{D} \nabla \rho(t, \xi)) \cdot \mathbf{n}_\Gamma(\xi) &= 0 & \text{for } \xi \text{ on } \partial\Omega \setminus \Gamma_{\text{top,right}} \end{aligned}$$

The diffusion tensor is given by $\mathbf{D} = \text{diag}([1, 0.5, 0.2])$ describing anisotropic diffusion. The nonlinearity is chosen as $f(\rho) = \rho/(1 + 0.5\rho)$, which is of the general form used to model saturating kinetics [16, 10]. The system is closed

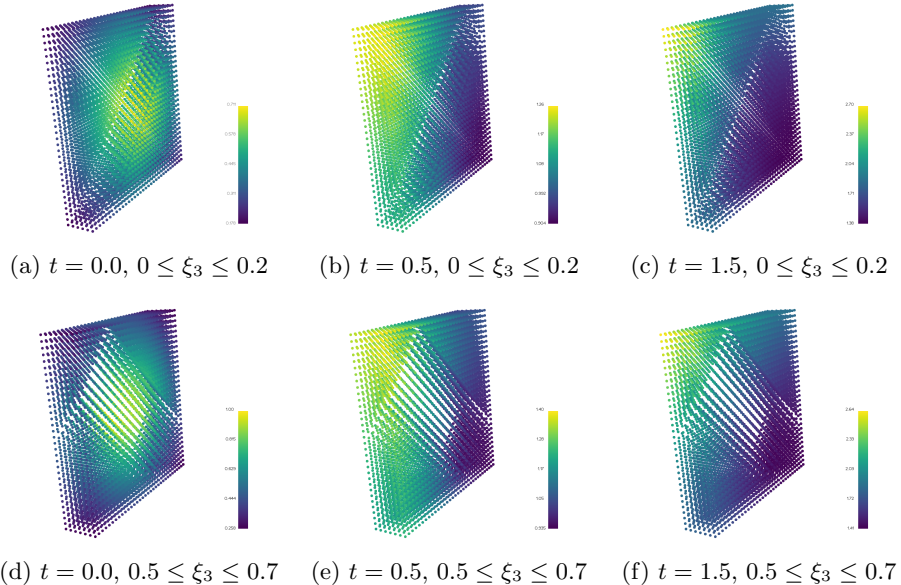


Fig. 2: Reaction-diffusion equation with $C = 0.75$: FOM solution visualized by slices of width 0.2 at different time points. (FOM with 163 840 cells.)

by initial conditions $\rho(0, \xi) = \rho_0(\xi; C)$ for $\xi \in \Omega$, where ρ_0 is varied over a parameter $C \in [0, 1]$, according to

$$\rho_0(\xi; C) = (1 - C) \exp\left(-\sum_{i=1}^3 \frac{(\xi_i - 0.5)^2}{0.1}\right) + C \exp\left(-\sum_{i=1}^3 \frac{(\xi_i - 0.5)^2}{0.5}\right)$$

for $\xi = [\xi_1, \xi_2, \xi_3] \in \Omega$. Similarly, the Neumann boundary conditions are varied according to

$$\begin{aligned} g_\Gamma(t, \xi; C) &= (1 - C) g_1(\xi) \sin(6t) + C g_2(\xi) \cos(4t) \\ \text{where } g_1(\xi) &= \sum_{i=1}^3 \xi_i, \quad \text{and} \quad g_2(\xi) = \sin(\xi_1) + \cos(6\xi_2)(0.3 - \xi_3^2). \end{aligned}$$

We refer to Fig. 2 for a visualization of the solution for the trajectory with $C = 0.75$.

The spatial discretization is carried out using the open-source Python library **scikit-fem**¹ [13], employing linear finite elements on a tetrahedral mesh with varying levels of refinement. The nonlinear term is integrated numerically using a four-point symmetric Gauss rule, meaning that the number of quadrature points in the FOM is four times the number of cells.

For all results, we use a ROM dimension of $N_r = 35$. The training of the POD basis and the empirical quadrature is carried out with snapshots from the training scenarios $C \in \{0, 0.5, 1\}$. By taking a snapshot every second time step, and since we employ a constant time step $\Delta_t = 0.002$, we obtain a total of 2253 snapshots for both the state and the nonlinearity.

Performance of standard vs. compressed training. As is shown in Fig. 3, our preprocessing significantly reduces memory requirements without noticeably affecting the fidelity of the reduced model for this example. The left part of the figure shows that the **standard training** contains approximately 40 000 equations, i.e., that amount of rows in the solution manifold matrix $\tilde{\mathbf{A}}$. The number of columns corresponds to the number of quadrature points. For the finest discretization shown in our results we have 1 533 520 quadrature points, which results in roughly 3 billion entries in the dense $\tilde{\mathbf{A}}$ and a memory requirement of 450 GB (assuming 8 bytes per entry). Thus, this setting and others are not treatable with the standard approach on a normal working station. In contrast, the **compressed training** reduces the number of equations to about 5%, and thus the memory requirements are reduced by a factor of 20.

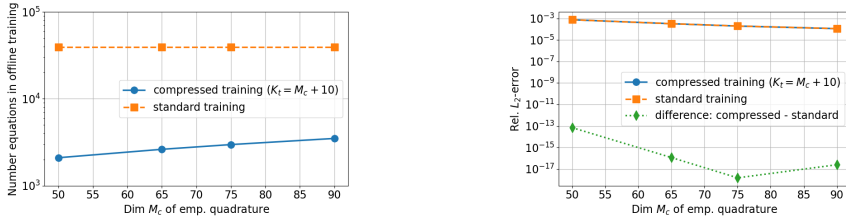


Fig. 3: Reaction-diffusion equation. Training performance for varying M_c , with and without compression. Left: Number of equations in offline training (independent of FOM dimension). Right: Relative space-time L_2 -errors of CRROM for the scenario with $C = 0.75$ and FOM with 56 025 cells.

In Fig. 4, we compare the offline training times for a varying number of cells in the FOM. For the two lowest dimensional FOMs, we see a gain of about one order. The third-lowest with about 56 025 cells is the largest, for which the **standard compression** does not run out of memory on our machine, and there we see a gain of two orders by our compression, i.e., about 10 000 seconds against 100 seconds training time.

¹<https://github.com/kinnala/scikit-fem/releases/tag/11.0.0>

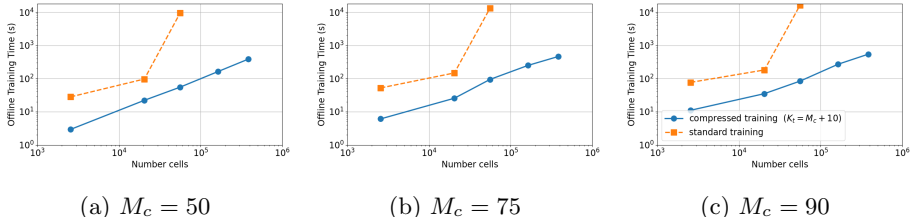


Fig. 4: Reaction-diffusion equation. Offline training times with and without compression, the varying number of cells in the FOM and M_c .

7.2. Gas transport network. The second example is based on the gas distribution network model [19], and it employs a mixed finite element discretization combined with a structure-preserving variant of POD for the model order reduction. We provide only a brief outline of the essential model and highlight only the details of the structure-preserving approximation that directly influence the complexity reduction, since all other details and chosen parameters can be found in [19]. We refer to [17] for the underlying FOM MATLAB code.

The network topology (Fig. 1-right) is adapted from the benchmark data set [23, GasLib-40], where compressors have been replaced by standard nodes. It comprises 38 pipes with diameters D^e ranging from 0.4 to 1 m and lengths l^e adding up to 1008 km in total. Each pipe is identified with an interval $[0, l^e]$, and the spatial domain Ω is defined as their union. The density and mass flux $\rho, m : [0, T] \times \Omega \rightarrow \mathbb{R}$ satisfy the Euler-type equations

$$(7.1) \quad \partial_t \rho + \partial_\xi m = 0, \quad \partial_t \frac{m}{\rho} + \partial_\xi \frac{m^2}{2\rho^2} + \partial_\xi P'(\rho) = -r(\rho, m) m,$$

where P' denotes the derivative of a pressure potential modeling an isothermal pressure law, and the friction term is given by $r : (\rho, m) \mapsto 0.008|m|/(2D^e\rho^2)$. The individual pipes are interconnected through energy-conservative coupling conditions enforcing continuity of the specific stagnation enthalpy and mass conservation. The system is closed by one boundary condition per boundary node and by initial conditions.

Apart from a refined spatial step size of $\Delta_\xi = 50$ m, we adopt the same parameters as in the reference. This choice yields 20 180 cells and a FOM dimension of $N = 40\,426$. The ROM dimension is splitted according to $N_r = N_{r,\rho} + N_{r,m} = 29 + 40$ on ROM states relating to ρ and m , respectively. We use $K = 2400$ snapshots for each of the three nonlinear terms in (7.1), which are uniformly distributed over the training trajectory described in [19]. More specifically, snapshots of the following mappings are collected:

$$(\rho, m) \mapsto \left(P'(\rho) + \frac{m^2}{2\rho^2} \right) \partial_\xi w_r^j, \quad (\rho, m) \mapsto r(\rho, m) m w_r^j, \quad (\rho, m) \mapsto \frac{m}{\rho} w_r^j,$$

for w_r^j with $j = 1, \dots, N_{r,m}$, which are piecewise linear ROM ansatz functions relating to m . Since the third nonlinearity appears as a time derivative, we

approximate it using finite differences. Our structured preprocessing method is applied to the snapshots of the first mapping, as well as to the union of the snapshots of the second and third mappings, where the latter is handled according to the simplified approach in (5.3).

Performance of standard vs. compressed training. For this example, the use of the **compressed training** yields a speedup of roughly a factor of four; for example, training with $M_c = 120$ cubature weights requires about 35 seconds with compression compared to approximately 140 seconds without, see Fig. 5-left. It can also be observed that **compressed training** times depend less on M_c , since the compression itself accounts for most of the computational effort.

The additional error introduced by compression is negligibly small, as can be seen by comparing the difference $\eta - \eta_t$ with the residual of the training η itself in Fig. 5-right. Moreover, the figure shows the strict a posteriori bound on η . This bound is not only computable in practice but also effective, as it results in an overestimation of only about one order of magnitude.

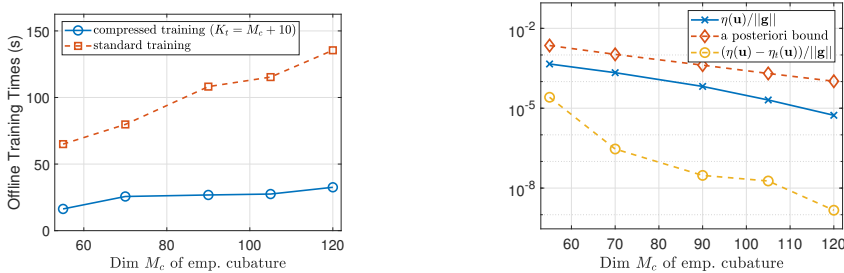


Fig. 5: Gas network. Comparison of training performance for varying M_c , with and without compression (using $K_t = M_c + 10$). Left: offline training times; right: training residuals, the difference introduced by compression, and the corresponding a posteriori bound from Theorem 6.1 (scaled by $\|\mathbf{g}\|$, where \mathbf{g} denotes the right-hand side of the training problem).

Conclusion and outlook. In this paper, we propose a preprocessing technique for empirical quadrature and other project-then-approximate complexity-reduction methods. The approach leverages structured data compression by exploiting the inherent structure of the training problems, thereby reducing memory requirements and offline training times by roughly an order of magnitude. This enables the application of such methods to larger-scale problems. The efficiency gains are demonstrated through numerical experiments, including tests that integrate our approach into the lightweight finite element library `scikit-fem`. Our focus is on model reduction for standard finite element discretizations.

Potential directions for future work include extending the approach to other and more general discretization settings and exploring algorithmic aspects such as efficient on-the-fly updates of the complexity reduction. Furthermore, it would be interesting to assess the performance of our method in highly parallelized environments, which are essential for very large-scale problems.

Acknowledgements. During the preparation of this work, the author used Microsoft Copilot available at <https://m365.cloud.microsoft/chat> to refine the language in certain parts of the manuscript. After using this tool, the author edited the content as needed and takes full responsibility for the content.

Availability of data. The data that support the findings of this study are available from the author upon reasonable request.

REFERENCES

- [1] B. Afkham and J. Hesthaven. Structure preserving model reduction of parametric Hamiltonian systems. *SIAM J. Sci. Comput.*, 39(6):A2616–A2644, 2017.
- [2] S. S. An, T. Kim, and D. L. James. Optimizing cubature for efficient integration of subspace deformations. *ACM Trans. Graph.*, 27(5):1–10, 2008.
- [3] T. Blumensath and M. E. Davies. Gradient pursuit for non-linear sparse signal modeling. In *2008 16th European Signal Processing Conference*, pages 1–5. IEEE, 2008.
- [4] J. Chan. Entropy stable reduced order modeling of nonlinear conservation laws. *J. Comput. Phys.*, 423:109789, 2020.
- [5] S. Chaturantabut and D. C. Sorensen. A state space error estimate for POD-DEIM nonlinear model reduction. *SIAM J. Numer. Anal.*, 50(1):46–63, 2012.
- [6] Z. Drmac and A. K. Saibaba. The discrete empirical interpolation method: Canonical structure and formulation in weighted inner product spaces. *SIAM J. Matrix Anal. Appl.*, 39(3):1152–1180, 2018.
- [7] E. Du and M. Yano. Efficient hyperreduction of high-order discontinuous galerkin methods: Element-wise and point-wise reduced quadrature formulations. *J. Comput. Phys.*, 466:111399, 2022.
- [8] C. Farhat, P. Avery, T. Chapman, and J. Cortial. Dimensional reduction of nonlinear finite element dynamic models with finite rotations and energy-based mesh sampling and weighting for computational efficiency. *Int. J. Numer. Meth. Eng.*, 98(9):625–662, 2014.
- [9] C. Farhat, S. Grimberg, A. Manzoni, and A. Quarteroni. *Computational bottlenecks for PROMs: precomputation and hyperreduction*, page 181–244. De Gruyter, 2020.
- [10] M. Frank, C. Lax, S. Walcher, and O. Wittich. Quasi-steady state reduction for the michaelis–menten reaction–diffusion system. *J. Math. Chem.*, 56(6):1759–1781, Feb. 2018.
- [11] G. H. Golub and C. F. Van Loan. *Matrix Computations*. The John Hopkins University Press, 3 edition, 1996.
- [12] S. Grimberg, C. Farhat, R. Tezaur, and C. Bou-Mosleh. Mesh sampling and weighting for the hyperreduction of nonlinear petrov–galerkin reduced-order models with local reduced-order bases. *Int. J. Numer. Methods Eng.*, 122(7):1846–1874, 2021.
- [13] T. Gustafsson and G. D. McBain. scikit-fem: A Python package for finite element assembly. *Journal of Open Source Software*, 5(52):2369, 2020.
- [14] J. Hernández, J. Bravo, and S. A. de Parga. Cecm: A continuous empirical cubature method with application to the dimensional hyperreduction of parameterized finite element models. *Comput. Methods Appl. Mech. Eng.*, 418:116552, 2024.
- [15] J. A. Hernandez, M. A. Caicedo, and A. Ferrer. Dimensional hyper-reduction of non-linear finite element models via empirical cubature. *Comput. Methods Appl. Mech. Engrg.*, 313:687–722, 2017.
- [16] K. A. Johnson and R. S. Goody. The original michaelis constant: translation of the 1913 michaelis–menten paper. *Biochem.*, 50(39):8264–8269, 2011.
- [17] B. Liljegren-Sailer. Code for the paper 'On port-Hamiltonian approximation of a non-linear flow problem on networks'. <https://doi.org/10.5281/zenodo.6372667>, 2022.
- [18] B. Liljegren-Sailer and N. Marheineke. On port-Hamiltonian approximation of a non-linear flow problem on networks. *SIAM J. Sci. Comput.*, 44, 2022.
- [19] B. Liljegren-Sailer and N. Marheineke. On snapshot-based model reduction under compatibility conditions for a nonlinear flow problem on networks. *J. Sci. Comput.*, 92(2), 2022.
- [20] T. T. Nguyen, J. Idier, C. Soussen, and E.-H. Djermoune. Non-negative orthogonal

greedy algorithms. *IEEE Transactions on Signal Processing*, 67(21):5643–5658, 2019.

[21] A. T. Patera and M. Yano. An l^p empirical quadrature procedure for parametrized functions. *C. R. Math.*, 355(11):1161–1167, Nov. 2017.

[22] R. Qu, A. Narayan, and J. Chan. Entropy stable reduced order modeling of nonlinear conservation laws. *Journal of Computational Physics*, 423:109789, 2020.

[23] M. Schmidt, D. Aßmann, R. Burlacu, J. Humpola, I. Joormann, N. Kanelakis, T. Koch, D. Oucherif, M. Pfetsch, L. Schewe, R. Schwarz, and M. Sirvent. GasLib – A Library of Gas Network Instances. *Data*, 2(4), 2017.

[24] Y. Takane and M. A. Hunter. Constrained principal component analysis: A comprehensive theory. *Appl Algebra Eng Commun Comput.*, 12(5):391–419, 2001.

[25] Y. Takane and T. Shibayama. Principal component analysis with external information on both subjects and variables. *Psychometrika*, 56(1):97–120, 1991.

[26] T. Wen and M. J. Zahr. A globally convergent method to accelerate large-scale optimization using on-the-fly model hyperreduction: Application to shape optimization. *J. Comput. Phys.*, 484:112082, 2023.